# Supporting Information

Sekhar et al. 10.1073/pnas.1212036109

## SI Materials and Methods

**Additional Details on Sample Preparation.** For each glycerol concentration, 100 mL of glycerol-containing buffer was made by mixing 50 mL of a twofold concentrated stock of NMR buffer with the requisite amount of glycerol, adjusting the pH to 5.7, and making up the volume to 100 mL with water. Then, 500 μL each of 0.7–1 mM wild-type (wt) or L24A FF domain stock solutions was dialyzed overnight against 100 mL buffer without or with glycerol using Midi (50–800 μL) 3.5-kDa molecular weight cutoff (MWCO) D-tube dialyzers (EMD Millipore). There is a decrease in sample volume upon dialysis for glycerol-containing samples that arises from osmotic effects, and this decrease is compensated by making up the sample to 500 μL with dialysis buffer. Samples containing BSA were prepared by diluting 500 μL of the wt FF or L24A FF stock solutions with NMR buffer, dissolving the necessary amount of BSA and concentrating the solution again to 500 μL. The samples were then dialyzed against NMR buffer to adjust pH and salt concentrations.

**Translational Diffusion Measurements of Acetate.** The diffusion coefficient of acetate was measured in NMR buffer as well as in wt FF and L24A FF domain samples without and with glycerol or BSA using a modified 1D water-sLED pulsed-field–gradient NMR pulse sequence (1). A relaxation delay of 20 s was used in these experiments to allow for complete longitudinal relaxation of the acetate magnetization between transients. Datasets were acquired at gradient strengths ranging between 4 and 30 G/cm using 2-ms gradients and a diffusion delay of 100 ms. The variation in the area under the acetate methyl $^1$H resonance at ∼1.9 ppm was evaluated as a function of gradient strength and fit to a single exponential decay. The decay constant obtained from the fit is linearly proportional to the sample-specific diffusion coefficient of acetate. The viscosities of the wt and L24A FF samples were then calculated using the inverse relationship between the diffusion coefficient and viscosity via the Stokes-Einstein equation. The viscosity of the NMR buffer was assumed to be identical to the concentration-weighted viscosities of $H_2O$ [90% (vol/vol)] and $^2H_2O$ [10% (vol/vol)] at the temperature of the experiment (2).

**Translational Diffusion Measurements of the wt FF Domain.** Translational diffusion coefficients of wt FF in NMR buffer and in samples containing glycerol were measured at 11.7 T, 30 °C using a $^1$H,$^{15}$N constant-time heteronuclear correlation-based pulse sequence (3). Heteronuclear single quantum coherence (HSQC) spectra were recorded with the position of molecules (along the $z$ axis) encoded using gradient strengths ranging from 4 to 30 G/cm applied for a duration of 1 ms, with a diffusion delay of 100 ms and a relaxation delay of 1.5 s. Peak intensities of ∼10 well-resolved correlations were quantified at each gradient strength and fit to a single exponential decay function to extract a diffusion decay constant.

**Estimating the Viscogen-Induced Change in the wt FF Domain Rotational Correlation Time.** The rotational correlation time of the wt FF domain was assumed to be proportional to fitted $^{15}$N $R_{2,eff}(\nu_{CPMG} = \infty) = R_{2,\infty}$ values measured from relaxation dispersion profiles. $^{15}$N dispersion curves were inspected, and 10 residues that did not undergo significant changes in $R_{2,eff}$ as a function of $\nu_{CPMG}$ were chosen for analysis. The residue-specific ratio $R_{2,\infty}$ (no viscogen)/$R_{2,\infty}$ (viscogen) = $\tau_C$(no viscogen)/$\tau_C$(viscogen) (where $\tau_C$ is the assumed isotropic rotational correlation time) was calculated and averaged over all 10 residues to give the fractional change in the rotational correlation time resulting from addition of viscogen.

**Error Estimation of Fitted Exchange Parameters Using a Bootstrap Analysis.** In addition to calculating errors in fractional populations of the intermediate state ($p_I$) and exchange rates ($k_{ex} = k_{IN} + k_{NI}$) from fits of relaxation dispersion profiles using a covariance matrix method (4), errors also have been estimated via a bootstrap analysis of all datasets (5). In this approach, dispersion profiles recorded at 11.7 and 18.8 T for residues listed in Tables S1–S3 were used in each analysis (separate analyses for each viscogen concentration, i.e., for each FF domain sample). Bootstrap datasets, $R_{2,eff}$ vs. $\nu_{CPMG}$, were generated by randomly choosing $R_{2,eff}$ data points from each experimental dispersion profile such that the total number of $R_{2,eff}$ values was kept constant. In this manner, some of the dispersion profiles will have repeat values of $R_{2,eff}$, with relaxation rates for certain $\nu_{CPMG}$ values missing (6). One thousand such bootstrap datasets were created for each glycerol or BSA concentration, with each dataset fit to a two-state exchange model, as described in the main text. For each sample, values of $p_I$ and $k_{ex}$ were segregated into 50 uniformly spaced bins and fit to a gaussian distribution, and the SD of the distribution in each case was assumed to be the error in the fitted parameters. Errors in $p_I$ and $k_{ex}$ were propagated to determine the errors in $\tau_I$ and $\tau_N$.

## SI Results and Discussion

**Exchange Parameters for the FF Domains Studied Here as Measured by Carr-Purcell-Meiboom-Gill (CPMG) Methods Are Not Correlated.** In some cases, the fitted values of $k_{ex}$, $p_I$, and $\Delta\varpi$ obtained from analysis of relaxation dispersion profiles can be correlated. For example, in the limit that $k_{ex} << \Delta\omega$ ($\Delta\omega$ is the difference in chemical shifts in rads per second) corresponding to slow exchange on the NMR chemical shift timescale (7), $p_I$ and $k_{ex}$ cannot be separated and only the product $p_I \times k_{ex}$ can be obtained from analysis of dispersion data. In contrast, for $k_{ex} >> \Delta\omega$ that is the fast exchange regime (7), $p_I$ and $\Delta\varpi$ are correlated in fits of data. In these cases, individual parameters cannot be estimated with confidence. In general, it is important to establish the robustness of the estimated exchange values, and we have done so for the FF domain systems considered here. Accurate exchange parameters are obtained from analysis of dispersion data when there is a wide distribution of exchange timescales that are sampled in a given dataset; that is, some of the residues are in fast exchange, some in slow exchange, and some also in the intermediate regime (8). This distribution may be quantified by calculation of an α parameter for each residue, defined by Millet et al. (9), that establishes how $R_{ex} = R_{2,eff}(\nu_{\mathrm{CPMG}} = 0) - R_{2,eff}(\nu_{\mathrm{CPMG}} = \infty)$ changes with static magnetic field strength, $B_o$,

$$\frac{d \ln R_{ex}}{d \ln B_o} = \alpha = \frac{2\left(\frac{k_{ex}}{\Delta\omega}\right)^2}{1 + \left(\frac{k_{ex}}{\Delta\omega}\right)^2}. \qquad [S1]$$

Values of 0 and 2 are obtained for the slow and fast chemical exchange cases, respectively, whereas for residues in the intermediate exchange regime, α values of ∼1 are calculated. Fig. S2 *A*–*E* illustrates the wide range of α values obtained for residues used in fitting exchange parameters (solid and open rectangles correspond to α at 11.7 and 18.8 T, respectively). It is clear that for each sample considered, there is a range of exchange rates, a prerequisite

for obtaining accurate (and uncorrelated) exchange parameters. This can be seen in Fig. S2 *F–J*, in which dispersion profiles for a pair of residues (recorded at 18.8 T) are highlighted, showing the different shapes that manifest in the diverse exchange regimes. Other lines of evidence exist that establish that the extracted parameters are not correlated. (*i*) Plots of $k_{ex}$ distributions obtained from the bootstrap analysis for the wt and L24A FF domains are shown in Fig. S3 along with fits to gaussian functions establishing that $k_{ex}$ for each sample decreases with increasing viscogen, as expected, with each profile distinguishable from that of its neighbors. If values of $k_{ex}$ were correlated with other extracted parameters, then random values of $k_{ex}$ as a function of viscogen might be found and most certainly not the smooth transition that is observed. (*ii*) Very similar $p_I$ values (identical to within experimental error) are obtained for samples of the same protein containing varying amounts of viscogen, which is possible only if the extracted fractional population values are not correlated with other parameters. (*iii*) Excellent agreement is obtained between extracted per-residue $\Delta\varpi$ values from samples with or without added viscogens for which different values of $k_{ex}$ are obtained (e.g., Fig. 3 and Figs. S4 and S5), consistent again with a lack of correlation between fitted parameters. The RMSD between $^{15}$N $\Delta\varpi$ values for samples without and with maximum concentrations of viscogen is 0.56, 0.20, and 0.18 ppm for wt FF + glycerol, wt FF + BSA, and L24A FF + BSA, respectively. (*iv*) Finally, previous studies demonstrated that robust exchange parameters may be obtained for exchanging systems with $p_I$ and $k_{ex}$ parameters in the range observed for wt and L24A FF without and with viscogens ($1 < p_I\,(\%) < 4.5$ and $500 < k_{ex}$ ($s^{-1}$) < 2,000) (8, 10, 11).


1. Altieri AS, Hinton DP, Byrd RA (1995) Association of biomolecular systems via pulsed field gradient NMR self-diffusion measurements. *J Am Chem Soc* 117(28):7566–7567.
2. Cho C, Urquidi J, Singh S, Robinson GW (1999) Thermal offset viscosities of liquid $H_2O$, $D_2O$, and $T_2O$. *J Phys Chem B* 103(11):1991–1994.
3. Choy WY, et al. (2002) Distribution of molecular size within an unfolded state ensemble using small-angle X-ray scattering and pulse field gradient NMR techniques. *J Mol Biol* 316(1):101–112.
4. Taylor JR (1997) *An Introduction to Error Analysis: The Study of Uncertainties in Physical Measurements* (Univ Science Books, New York).
5. Efron B, Tibshirani R (1986) Bootstrap methods for standard errors, confidence intervals, and other measures of statistical accuracy. *Stat Sci* 1(1):54–75.
6. Choy WY, Zhou Z, Bai Y, Kay LE (2005) An 15N NMR spin relaxation dispersion study of the folding of a pair of engineered mutants of apocytochrome b562. *J Am Chem Soc* 127(14):5066–5072.
7. Cavanagh J, Fairbrother WJ, Palmer AG, Rance M, Skelton NJ (2007) *Protein NMR Spectroscopy: Principles and Practice* (Academic, New York), 2nd Ed.
8. Hansen DF, Vallurupalli P, Lundström P, Neudecker P, Kay LE (2008) Probing chemical shifts of invisible states of proteins with relaxation dispersion NMR spectroscopy: how well can we do? *J Am Chem Soc* 130(8):2667–2675.
9. Millet O, Loria JP, Kroenke CD, Pons M, Palmer AG III (2000) The static magnetic field dependence of chemical exchange linebroadening defines the NMR chemical shift time scale. *J Am Chem Soc* 122(12):2867–2877.
10. Loria JP, Rance M, Palmer AG III (1999) A relaxation-compensated Carr-Purcell-Meiboom-Gill sequence for characterizing chemical exchange by NMR spectroscopy. *J Am Chem Soc* 121(10):2331–2332.
11. Korzhnev DM, Religa TL, Banachewicz W, Fersht AR, Kay LE (2010) A transient and low-populated protein-folding intermediate at atomic resolution. *Science* 329(5997): 1312–1316.

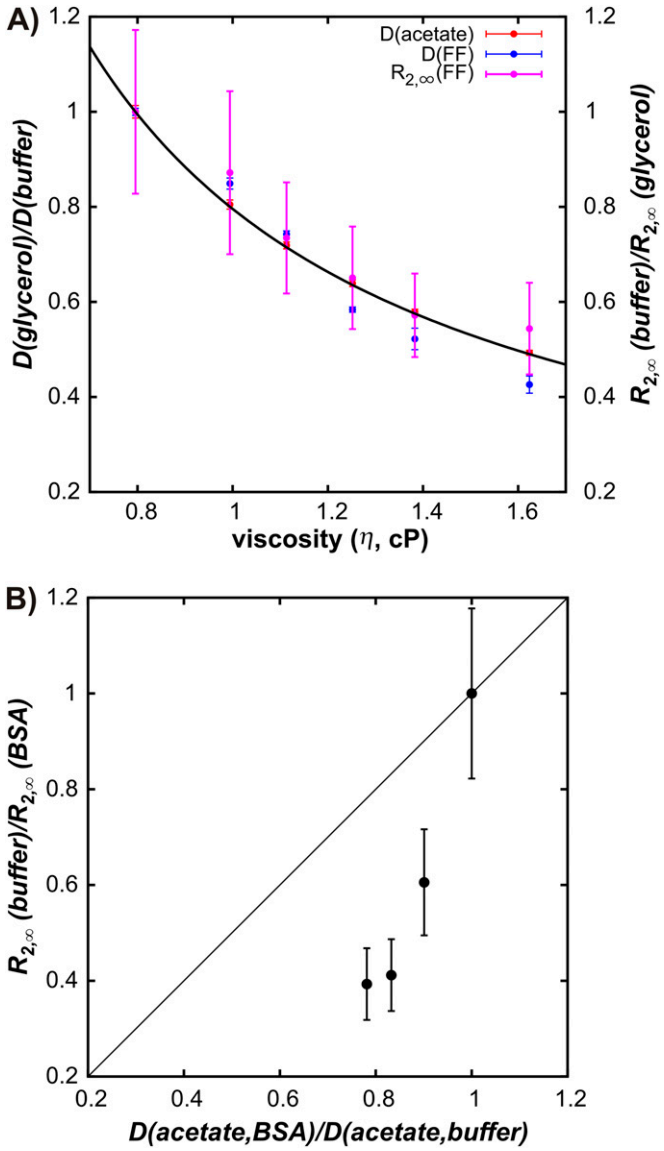


**Fig. S1.** Comparison of the influence of glycerol and BSA on the diffusion of acetate and the FF domain (30 °C). (*A*) Translational diffusion coefficients of acetate and wt FF normalized to the corresponding values in buffer (left *y* axis) and ratios of $R_{2,\infty}$ values (proportional to correlation times) of protein as measured in buffer and glycerol (right *y* axis) as a function of solvent viscosity, 30 °C. The solid line is the function $y = 0.8/x$ (ordinate is normalized to 1 in buffer without glycerol, $\eta_o$ = 0.8 cP at 30 °C). (*B*) $R_{2,\infty}$ ratios, as described in (*A*), for wt FF domain (*y* axis) vs. ratios of acetate diffusion coefficients (*x* axis) in samples containing different amounts of BSA, 25 °C. The solid line is $y = x$. The rotational correlation time and the translational diffusion coefficient of the wt FF domain were measured as described in *SI Materials and Methods*.

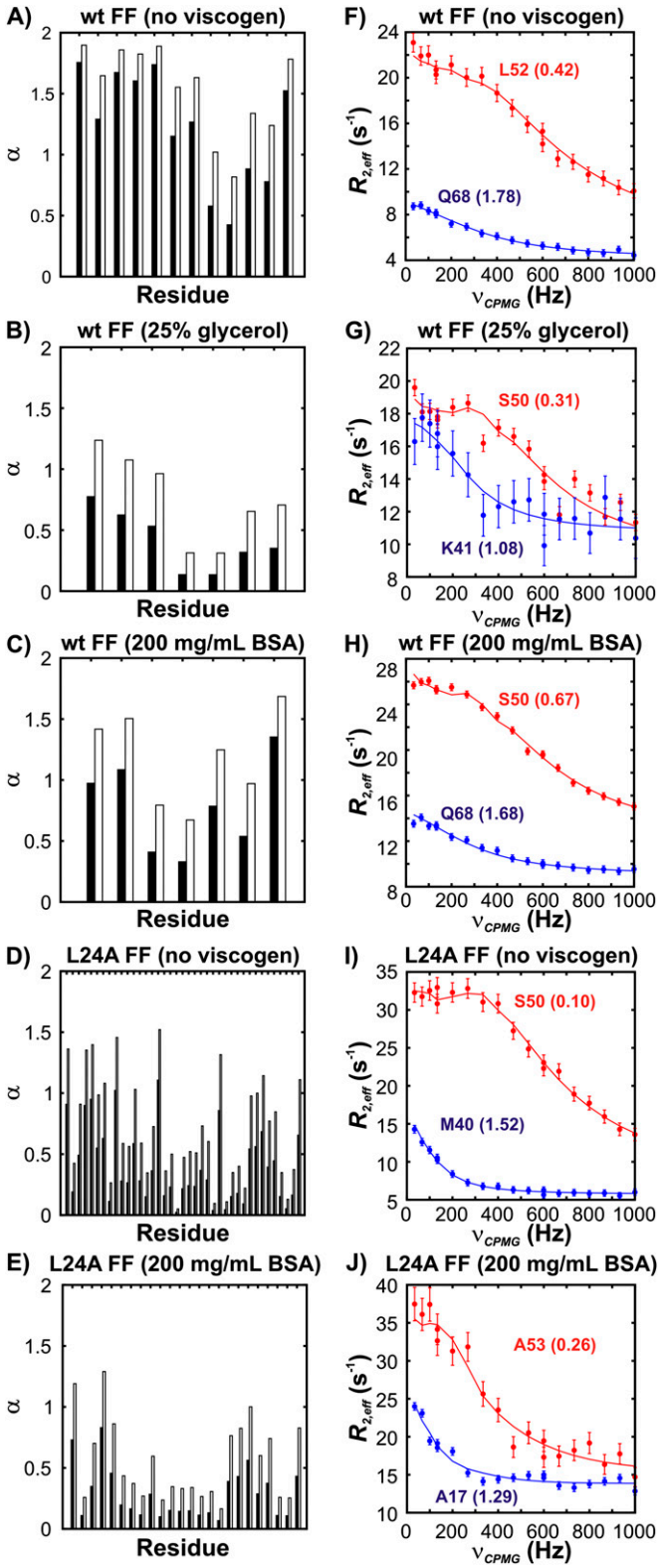


**Fig. S2.** Chemical exchange in the FF domain covers a range of timescales, from slow to moderately fast. (*A–E*) Distribution of α values (open and closed rectangles correspond to α values calculated at 11.7 and 18.8 T, respectively; see *SI Results and Discussion* for a definition of α) for residues used in global fits of dispersion data to obtain lifetimes and intermediate-state populations. Shown also are representative $^{15}$N dispersion profiles (*F–J*) for wt FF in (*F*) the absence of viscogen, (*G*) the presence of 25% (vol/vol) glycerol, or (*H*) 200 mg/mL BSA. (*I* and *J*) Profiles from the L24A FF domain recorded in the absence (*I*) or presence (*J*) of 200 mg/mL BSA. The α value at 18.8 T is indicated within parentheses for the residues whose dispersions are shown in *F–J*.

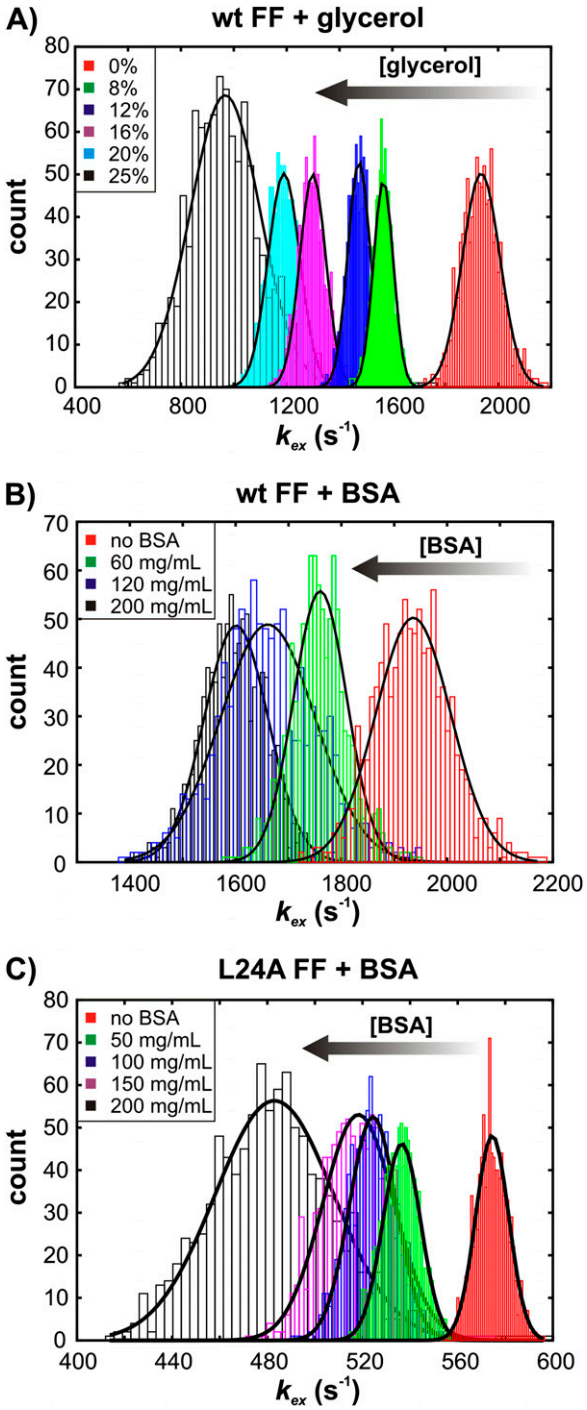


**Fig. S3.** Distribution of FF domain exchange rates as a function of added viscogen. Range of obtained $k_{ex}$ values for (*A*) wt FF in glycerol, (*B*) wt FF in BSA, and (*C*) L24A FF in BSA generated via a bootstrapping procedure described in *SI Materials and Methods*. The values of the distribution in each case are sorted into 50 equally sized bins, which accounts for the different bin sizes between samples. Solid lines represent fits of the binned distributions to gaussian functions. Small variations in the width of the distributions arise from several factors, such as differences in sample concentration and hence signal to noise and the magnitude of $R_{ex}$.

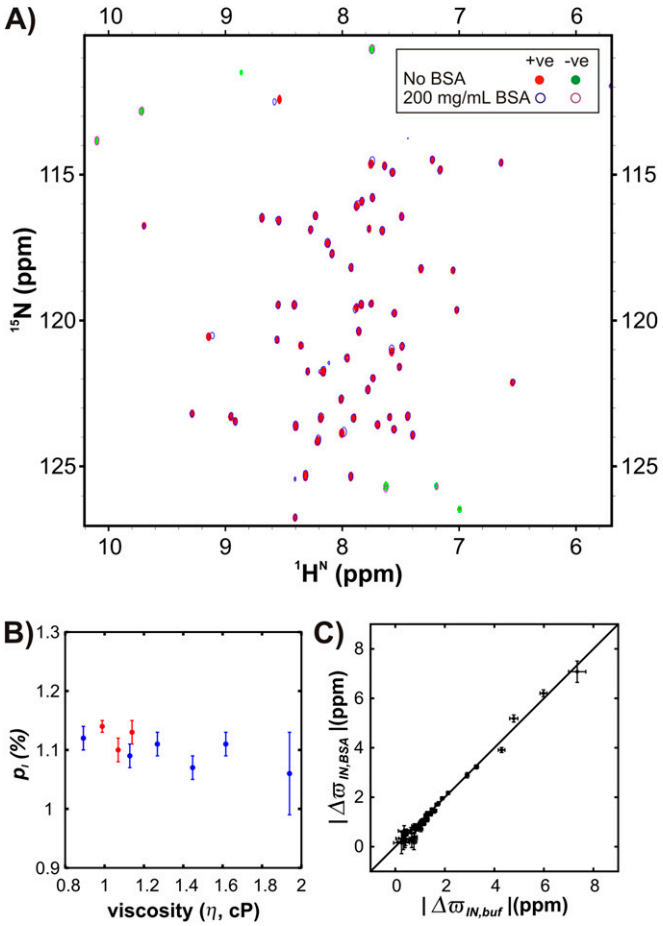


**Fig. S4.** BSA does not perturb the structures of intermediate (I) and native (N) states of the wt FF domain or their relative energies. (*A*) Overlay of $^{1}$H,$^{15}$N HSQC spectra of the wt FF domain acquired without and with 200 mg/mL BSA. Correlations that are aliased in $F_1$ are plotted in green (no BSA) or purple (200 mg/mL BSA). (*B*) $p_I$ values as a function of solvent viscosity in BSA (red) and glycerol (blue). The data point without viscogen is common to both datasets. (*C*) Comparison of $|\Delta\varpi_{IN}|$ values in the absence (*x* axis) and presence (*y* axis) of 200 mg/mL BSA. The straight line graphs $y = x$.

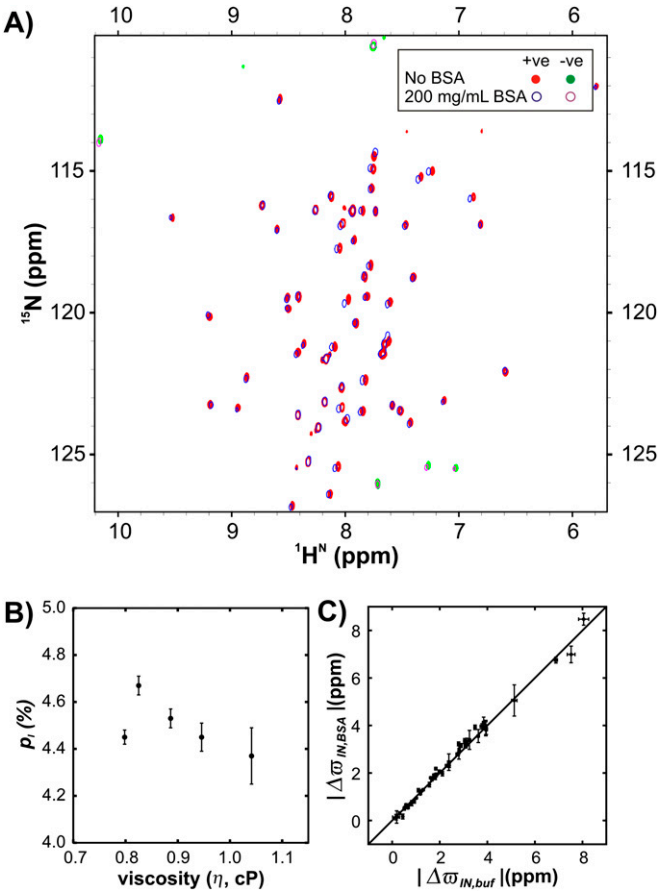


**Fig. S5.** BSA does not perturb the structures of L24A FF N and I or their energies. (*A*) Overlay of $^{1}$H,$^{15}$N HSQC spectra of L24A FF acquired without and with 200 mg/mL BSA. Correlations that are aliased in $F_1$ are plotted in green (no BSA) or purple (200 mg/mL BSA). (*B*) $p_I$ values as a function of solvent viscosity. (*C*) Comparison of $|\Delta\varpi_{IN}|$ values in the absence (*x* axis) and presence (*y* axis) of 200 mg/mL BSA. The line $y = x$ is shown.

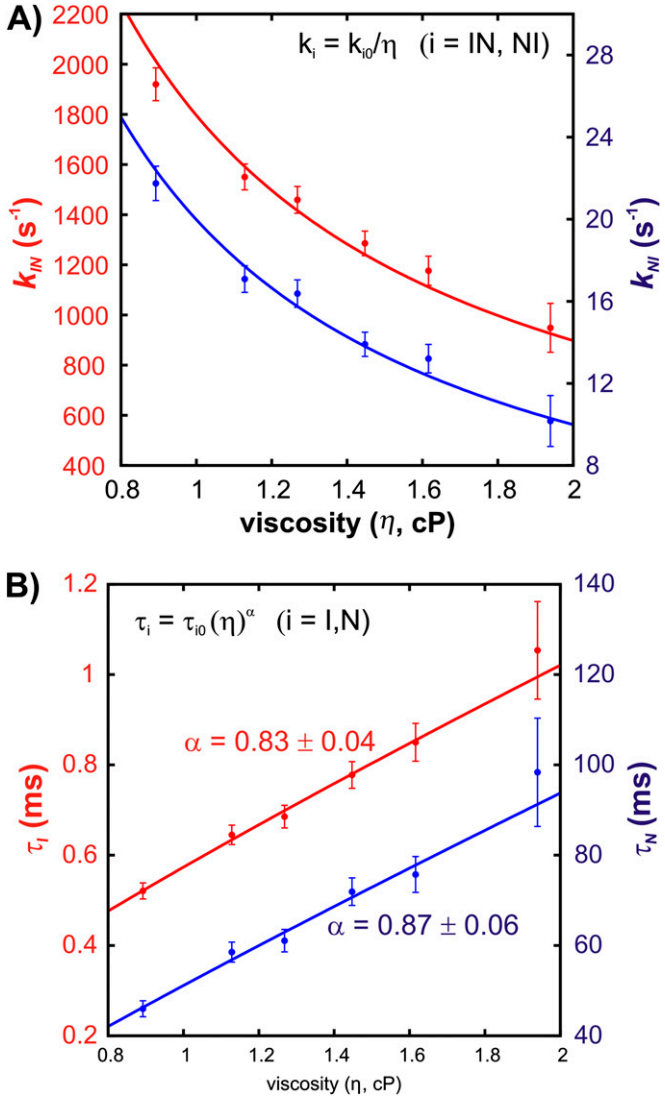


**Fig. S6.** Exchange rates for the interconversion between intermediate and native states of the wt FF domain, 25 °C, can be well fit to a power law viscosity equation (1). (*A*) Viscosity-dependent rate constants, $k_{IN}$ and $k_{NI}$, of the wt FF domain. Solid lines are fits of the data to a function of the form $k_i = \frac{k_{i0}}{\eta}, (i \in IN, NI)$. (*B*) Intermediate- and native-state lifetimes of the wt FF domain, 25 °C, as a function of viscosity. Solid lines are best fits of the data to a power law equation of the form $\tau_i = \tau_i 0 \eta^{\alpha}, (i \in I, N)$. The α value obtained from the fitting routine is indicated on the graph. Values close to 1 indicate that the viscosity dependencies of the rates derive predominantly from the effects of solvent friction. This conclusion also follows from fits of rates to Eq. **3** of the text, where σ values significantly smaller than 1 are obtained. Solution viscosities were modified by addition of varying amounts of glycerol, as described in the text.

1. Jas GS, Eaton WA, Hofrichter J (2001) Effect of viscosity on the kinetics of α-helix and β-hairpin formation. *J Phys Chem B* 105:261–272.

**Table S1. Exchange kinetics for wt FF in the presence of glycerol**

| | | | | Covariance matrix method* | | | Bootstrap analysis† | | |
|---|---|---|---|---|---|---|---|---|---|
| Glycerol, % (vol/vol) | Viscosity, cP | Dispersions fit, *n* | $\chi^2_{red}$ | $p_I$, % | $\tau_I$, ms | $\tau_N$, ms | $p_I$, % | $\tau_I$, ms | $\tau_N$, ms |
| 0 | 0.89 | 12 | 0.8 | 1.12 ± 0.02 | 0.52 ± 0.02 | 46 ± 2 | 1.13 ± 0.03 | 0.52 ± 0.02 | 46 ± 2 |
| 8 | 1.13 | 10 | 0.5 | 1.09 ± 0.02 | 0.64 ± 0.02 | 58 ± 2 | 1.10 ± 0.01 | 0.64 ± 0.02 | 58 ± 2 |
| 12 | 1.27 | 10 | 0.6 | 1.11 ± 0.02 | 0.68 ± 0.02 | 61 ± 2 | 1.11 ± 0.02 | 0.69 ± 0.02 | 61 ± 2 |
| 16 | 1.45 | 8 | 0.8 | 1.07 ± 0.02 | 0.78 ± 0.03 | 72 ± 3 | 1.07 ± 0.02 | 0.78 ± 0.03 | 72 ± 3 |
| 20 | 1.62 | 7 | 1.0 | 1.11 ± 0.02 | 0.85 ± 0.04 | 76 ± 4 | 1.11 ± 0.03 | 0.85 ± 0.04 | 76 ± 4 |
| 25 | 1.94 | 7 | 1.1 | 1.06 ± 0.07 | 1.05 ± 0.11 | 98 ± 12 | 1.13 ± 0.03 | 1.04 ± 0.14 | 91 ± 13 |

*Errors in the parameters are estimated using the covariance matrix method.
†Errors in the parameters are estimated by a bootstrap analysis as detailed in *SI Materials and Methods*.

**Table S2. Exchange kinetics for wt FF in the presence of BSA**

| | | | | Covariance matrix method* | | | Bootstrap analysis† | | |
|---|---|---|---|---|---|---|---|---|---|
| BSA, mg/mL | Viscosity, cP | Dispersions fit, *n* | $\chi^2_{red}$ | $p_I$, % | $\tau_I$, ms | $\tau_N$, ms | $p_I$, % | $\tau_I$, ms | $\tau_N$, ms |
| 0 | 0.89 | 12 | 0.8 | 1.12 ± 0.02 | 0.52 ± 0.02 | 46 ± 2 | 1.13 ± 0.03 | 0.52 ± 0.02 | 46 ± 2 |
| 60 | 0.99 | 12 | 0.8 | 1.14 ± 0.01 | 0.57 ± 0.02 | 50 ± 2 | 1.15 ± 0.01 | 0.57 ± 0.02 | 49 ± 2 |
| 120 | 1.07 | 8 | 1.3 | 1.10 ± 0.02 | 0.60 ± 0.02 | 54 ± 2 | 1.10 ± 0.03 | 0.61 ± 0.03 | 55 ± 3 |
| 200 | 1.14 | 7 | 1.1 | 1.13 ± 0.02 | 0.63 ± 0.02 | 55 ± 2 | 1.13 ± 0.02 | 0.63 ± 0.02 | 55 ± 2 |

[a]Errors in the parameters are estimated using the covariance matrix method.
†Errors in the parameters are estimated by a bootstrap analysis as detailed in *SI Materials and Methods*.

**Table S3. Exchange kinetics for L24A FF in the presence of BSA**

| | | | | Covariance matrix method* | | | Bootstrap analysis† | | |
|---|---|---|---|---|---|---|---|---|---|
| BSA, mg/mL | Viscosity, cP | Dispersions fit, *n* | $\chi^2_{red}$ | $p_I$, % | $\tau_I$, ms | $\tau_N$, ms | $p_I$, % | $\tau_I$, ms | $\tau_N$, ms |
| 0 | 0.80 | 39 | 1.1 | 4.45 ± 0.03 | 1.82 ± 0.02 | 39.0 ± 0.5 | 4.45 ± 0.04 | 1.82 ± 0.02 | 39.1 ± 0.6 |
| 50 | 0.82 | 38 | 1.1 | 4.67 ± 0.04 | 1.95 ± 0.02 | 39.8 ± 0.6 | 4.67 ± 0.05 | 1.96 ± 0.03 | 39.9 ± 0.7 |
| 100 | 0.89 | 39 | 1.2 | 4.53 ± 0.04 | 1.99 ± 0.03 | 41.8 ± 0.7 | 4.54 ± 0.06 | 2.00 ± 0.04 | 42.0 ± 1.0 |
| 150 | 0.95 | 34 | 1.2 | 4.45 ± 0.06 | 2.02 ± 0.04 | 43.4 ± 1.0 | 4.45 ± 0.08 | 2.02 ± 0.06 | 43.4 ± 1.5 |
| 200 | 1.04 | 24 | 1.1 | 4.37 ± 0.12 | 2.18 ± 0.08 | 47.6 ± 2.2 | 4.36 ± 0.15 | 2.16 ± 0.11 | 47.5 ± 3.0 |

*Errors in the parameters are estimated using the covariance matrix method.
†Errors in the parameters are estimated by a bootstrap analysis as detailed in *SI Materials and Methods*.